Твердотельная электроника

I.E. Matyash[1], Ph.D., **I.A. Minaylova**[1], **O.N. Mischuk**[1], Ph.D., **O.O. Oliinyk**[2], **B.K. Serdega**[1], Dr.Sc., **B.A. Tsyganok**[2], Ph.D.

[1]Lashkarev Institute of Semiconductor Physics, NAS of Ukraine, pr. Nauky 45, Kyiv, 03028, Ukraine,
[2]National Technical University of Ukraine "KPI", pr. Peremogy 37, Kiev-56, 03056, Ukraine.

Detection of stresses induced by heat flux in a solid by using a photo-elastic microscope

The aim of this paper is to present adventures of practical and effective modulation polarimetry method (MPM) applied to the plate sample of quartz glass for detection of its minute internal thermoelastic stresses induced by heat wave propagation. Described MPM allowed to make accurate measuring of birefringence that accompany the dynamics of thermoelasticity and made possible to calculate the value of stress distribution along and crosswise to the direction of heat flow at certain moments of time, as well as its dependence on time in defined heat flux coordinates. The main goal of this paper is not only the solution of inverse problems of nonstationary thermoelasticity that allowed obtaining spatio-temporal temperature functions by graphical integration of the experimental characteristics but researching the dynamics of the maximum curvature point of the temperature function T(t) that is a characteristic of the thermal front in the process of heat flow establishment. In addition, it is shown that due to the high detectability of MPM applied in photoelastic microscope became possible to observe the radiation component of the heat transfer process. References. 20, figures. 5.

Keywords: *modulation polarimetry, birefringence, heat flow, thermoelastisity, photoelastic microscope.*

1. Introduction

The combination of heat-conducting media sets, the mechanisms of heat transfer and the conditions with respect to linearity of heat conductivity coefficients in their equation generates almost an inexhaustible set of effects, associated with the thermoelastisity in solid state physics and their practical applications. Therefore, despite the long history of the problem [10,19], the interest to internal mechanical stress, linked to the heat transfer, judging by the ongoing publications does not decline.

Thermoelastic stress analysis is relatively new method and involves structures and materials under both mechanical and thermal loadings starting from nanoscale and is not limited in maximum dimensions. A universal nature of thermoelasticity (so-called "second sound" effect) gives many advantages in applications to variable objects [10]. A radiometer was used to record thermoelastic response in first analysis [15]. The first commercial thermoelastic stress analysis instrument was designed and developed [7] for fundamental thermoelastic researches [7,11] that revealed the thermoelastic method possibilities in composites, damage assessment, fracture mechanics and other applications [9,11,14-15]. Most solids exhibit a dimensions change with temperature variation, and thus the presence of a heat flux induces stresses, which can be sufficiently high when temperature variation is high, these stresses can reach levels that may lead to structural failure, especially for brittle materials. Thus, for many problems involving nondestructive control and diagnostic at high and low temperature gradients, the knowledge of thermal stress analysis can be very important. For solving these problems a wide range of methods are already developed, the main are ultrasound, Raman spectroscopy, X-Ray and neutron diffraction, holographic interferometry, conventional optical polarimetry methods [12], recently developed digital image correlation methods for planar surface displacement and strain/stress measurement [2] are very promising but still need a lot of improvements. Starting from 1999 a Stress Photonics have been formed as a scientific direction and uses photoelastic, thermoelastic and thermal nondestructive evaluation methods to complete a full line of full-field stress and strain measurement instruments. A lot of especial attention is paid for researching the possibility of thermoelastic effect for diagnostic of mechanical stresses in solids [3]. There are a lot of experimental results for metals and ceramics [3] that approve the informational capacity of presented effect. The influence mechanisms of mechanical stresses on the results of laser thermoelastic measurements are still not well established. The model of thermoelastic signal as a function of me-

chanical stresses [3], shows dependence on thermophysical material parameters.

Thermal and thermoelectric transport in nanometer scale devices and structures has become one of the nanotechnology focuses. The length scale is comparable to the scattering free paths of electrons and phonons. As a result, nanocomponents exhibit unique electron and phonon transport phenomena that have not been observed in micron-scale devices. For example, the effective thermal conductivity of the structure is drastically reduced due to increased phonon-boundary scattering. These effects combine to cause localized self heating and elevated operating temperatures that can reduce device speed and time to failure. A variety of nanoscale devices and structures are being actively developed for electronics, optoelectronics, thermoelectrics, electromechanical, sensing applications and all they are miniaturized that cause power density increasing. Examples include nanoelectronic devices based on carbon nanotubes, nanolasers based on ZnO nanowire arrays, thermoelectric coolers based on superlattices and nanowires, nanosensors based on carbon nanotubes, Si nanowires, and metal oxide nanobelts. All these components are studied by modern scanning thermal and thermoelectric microscopy that allowed to scan only surface thermoelastisity and gave no information about internal structure [20]. However, almost all modern optical methods are unable to universal thermoelastic research of internal structure from nano- and microelements to bulk materials with adaptive resolution, scan speed and sensitivity, also are characterized by varying degrees in certain information limitation, which under the presence of a distinguished set dictates the search for new effects and the creation of new methods on their basis which satisfy the needs of physicists and engineers.

From this point of view, it seems strange that the thermoelastic and photoelastic effects are ignored in practices of the investigation of thermal conductivity features. The essence of registration of both effects lays in the measurement of induced birefringence in an isotropic material under the action of an external or internal directed force (nonuniform potential). In [15] as regards this subject, is noted that the registration of the optical anisotropy is a very sensitive method of stress monitoring in transparent bodies and demonstrates the application examples.

However, thermal stresses and, consequently, the optical anisotropy are accompanied not only by the thermal pulses, but by stationary heat flux under the condition $\mathrm{div}\left(\mathrm{grad}\,T\right) \neq 0$, where T is the spatial function of temperature. Perhaps, the small absolute values of appeared stress/strain (deformation) and its corresponding birefringence in conditions of low temperature fluctuations is the cause that limits the application of optical methods in the research of thermoelasticity. Indeed, as shown in several papers, for example in [4], the conditions for half-wave plate, as a measure of mechanical stress/strain in ordinary optical-polarization method, the required gradients and, consequently, the temperature differences of values in which not only the thermal conductivity, but other parameters of the substance become a spatio-temporal function.

Taking into account these problems the goal of this work is experimental confirmation of the established theoretical relationship between the distribution of temperature and mechanical stress on the example of a sample of fused quartz. To achieve this goal a photoelastic microscope was used, which was designed and built based on the method of polarization modulation and allows precise measurements of changes in the refractive index and the Stokes parameters of the probe radiation with high detectivity. On the basis of obtained results, it is possible to calculate the temperature field and thermal stress not only in the model sample, but also in the component base of electronic equipment.

The task of the paper is obtaining the experimental confirmation of the functional relationship between temperature field and accompanying thermal stress on the base of theoretical features of photoelastic and thermoelastic effects [7,10-11,13] with considering the results summarized in [18] and using the technique of polarization modulation implemented in photoelastic microscope [16].

2. Experimental setup for photoelastic microscopy

The essence of the classical technique modification lays in that fact that the modulator of polarization of electromagnetic radiation is added to the optical-polarization device of the traditional implementation. The need for this addition is being dictated by two factors.

The first factor is that the non-polarized component for various reasons is always present in varying degrees in radiation. It is well known that the state of polarization has a large information capacity relatively to the anisotropic properties of the objects [18]. However, a non-polarized component, while not being linked with them, plays a limiting

role in their detection, made, as a rule, by the intensity modulation technique.

For exposition of the second circumstance it is necessary to clarify the term "state of polarization" that has several definitions. In this case the definition based on the Stokes parameters is used, namely $S = \begin{bmatrix} I & Q & U & V \end{bmatrix}$, where Q and U are two linear and V is a circular component in the accepted signs [18]. In the case of the polarization modulation a periodic change of its state takes place at a constant intensity. As a result, the signal, linked with a polarized component is separated in the recording device from the general signal, allowing gaining it by orders of magnitude.

The second factor is divided into two parts and is connected with the placement of PM in the optical system. Thus, the location of the PM at the front of the sample used in schemes for the study of the amplitude anisotropy is a reflection or a transmission [18]. If the PM is placed behind the sample, being in a block with a linear polarizer, it plays the role of the dynamic analyzer of polarization state of the radiation passed through the sample. The need for this procedure lies in the fact that the linearly polarized in initial state radiation, propagating through the studying object is converted in general case into elliptically polarized components. The magnitude of the circular component in its composition is given by $I_V \approx \sin(\varphi)\sin(\omega t)$ [18]. Here ω is the frequency of modulation; φ is a phase difference of orthogonal linear components of the radiation passed through the sample with thickness d, which in the coordinates of Fig.1 (b) is defined by [20];

$$\varphi = \varphi_x - \varphi_y = \frac{2\pi}{\lambda} d\left(n_x - n_y\right), \qquad (1)$$

n_x, n_y – the refractive indices of the sample material, which depend on the magnitude and sign of the strain/stress in the direction of the corresponding axes.

If the value of the optical anisotropy is $\varphi < 1$, the detected signal from the passed radiation is expressed by the value of the V component, which is a direct measure of internal mechanical strains/stresses. The optical setup shown in fig. 1 (a) is built just according to this case and is used in this study is.

A semiconductor laser is used as a source of radiation with a wavelength $\lambda = 650$ nm and a low level of optical noise. The role of the linear polarizer on the way of emitted radiation is "cleaning" components from the circular which are not related to the properties of the sample.

The axis of the polarizer and, consequently, the direction of the wave field $\overline{E}$ must form a certain angle relatively to the axes of the ellipsoid of wave normals [18] of the studied object at which the linearly polarized radiation is optimally converted to circular. This means that the stresses or deformations coursed by directed force that create the optical anisotropy in initially isotropic material are optically detected. Since the deformation caused by the thermal stresses is associated with the direction of the temperature gradient (heat flux Q), the azimuth of the electric field $\overline{E}$ of the wave in the initial state is reasonable to be set at an angle of 450 relatively to the optical axis of the sample, see Fig.1 (b), so that $E_x = E_y$. In this case, having reached the anisotropy $\varphi = \varphi_x - \varphi_y = 90°$ for any reason, all the radiation becomes circularly polarized, and the sample acquires the properties of the quarter-wave plate.

The polarization modulator is a dynamic phase plate [18], in which an optical anisotropy is created by periodic compression-tension from the attached cavity made of crystalline quartz. The functioning of the photoelastic modulator as an element, which controls the polarization state, is discussed in details in [4,20]. Moreover, there it can be shown that the signal of photodetector in the general case of elliptically polarized light could be factorized into linear and circular components. The base for expansion is a formalism that describes the process of modulation, according to which the circularly and linearly polarized radiations generate variable signals of photodetector at the frequency of the cavity and at the double frequency, respectively.

a)

b)

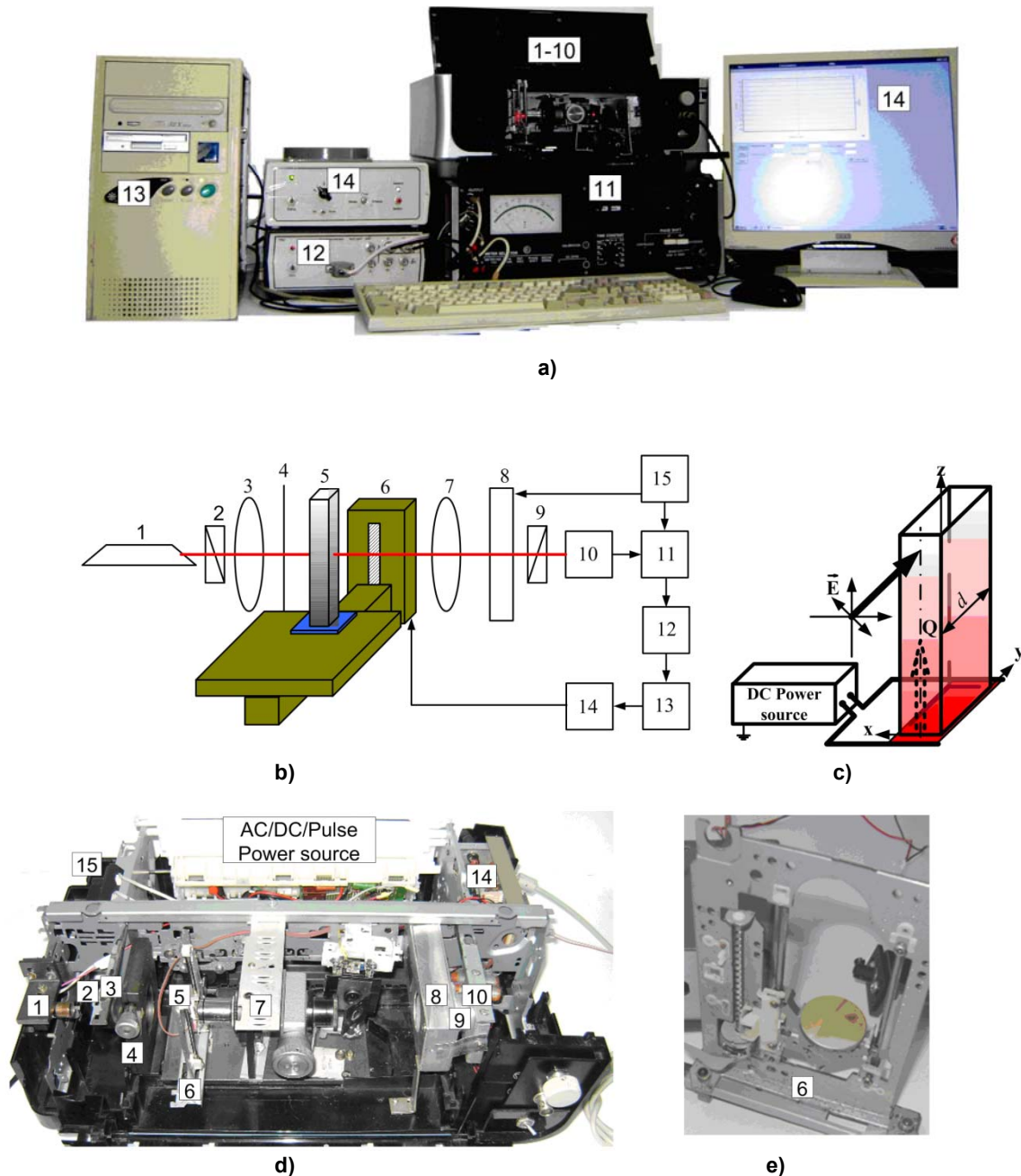
c)

d)

e)

Fig. 1. The experimental setup (a), block-diagram of the experimental setup (b), (c) shows the condition of the experiment, internal structure of photoelastic microscope (d), submicron positioning system based on stepper motor (e), where 1 is a laser diode, 2 is a polarizer, 3 is a lens, 4 is a compensating quarter-wave plate, 5 is a sample, 6 – positioning system, 7 is a micro objective, 8 is a photoelastic modulator, 9 is a PM-analyzer, 10 is a photodetector, 11 is a lock-in-nanovoltmeter, 12 – ADC, 13 – PC, 14 – stepper motor control unit, 15 is a power supply unit of the polarization modulator; $\vec{E}$ – wave's electric field, Q – heat flux, d – length of the sample

Taking into account earlier described specific of laser radiation parameters influence on the output signal a method [17] and device [16] has been developed for photoelastic microscopy of solids and their structures. Where the input function is the wave $\vec{E}(\theta,t)=\overline{E_0}e^{i(\omega t+kz)}$, in which the azimuth of field E_θ is set at an angle $\theta=45^0$ relative to optical indicatrix axes of the dielectric properties of the sample. Note that under $\theta=45^0$ equality holds $E_{0x}=E_{0y}$, due to what a phase difference is achieved during wave propagation in anisotropic

substance $\varphi_x - \varphi_y = \Delta = \pi / 2$ it becomes circularly polarized, this difference is caused according to the equation (1). The use of certain initial state of wave polarization ($\theta = 45^0$) the measurement principle of polarization state value is implemented, the effectiveness of which lays in registering the useful signal that has a circularly polarized component of the radiation, which was absent in the initial state of and whose appearance is caused by anisotropy. The dependence of the circular components of the radiation I_{out} on the anisotropy value $\Delta = \varphi_x - \varphi_y$, and on the intensity of the input radiation I_{in} according to the calculation method of matrix optics characterized by the ratio:

$$I_{out} = \frac{I_{in}}{2}\left[1 - \sin[\sin\Delta]\delta_0 \sin(\Omega t)\right], \qquad (2)$$

where δ_0 - value of phase shift of the polarization modulator, Ω - modulation frequency. Granted $\Delta < 1$ and limiting to the first term of the expansion in a series of Bessel functions we obtain a simplified expression intensity falling on the photodetector:

$$I_{out} \cong \frac{I_{in}}{2}\left[1 + \Delta\delta_0 \sin(\Omega t)\right]. \qquad (3)$$

In present paper a variable component of the signal presents interest that is measured by photoelastic microscope on the modulation frequency Ω =50 kHz and reflects the magnitude of the circular components of the radiation - $V = 2E_x E_y \sin\Delta$.

2.1. Noise and errors of measurements

To estimate the parameters of quasi-determined signals consider the problem of parameter A estimation in informative signal $x(t)$ as $x(t) = A \cdot u(t)$, where $u(t)$ - known function of time that describes the shape of the signal from the background noise with spectral density $W(j\omega)$. The input signal $z(t)$, which is an additive mixture of signal $x(t)$ and noise, is multiplied by the reference signal $u(t)$ of generator during the time interval $(0; t_0)$, is averaged by integrator and increased. The output variable of the filter is estimation of A parameter of signal $x(t)$. This signal $u(t)$ defines a linear filter impulse response of linear estimation that must match with the shape of valid signal. For linear estimation of signal parameters on uncorrelated noise background the formula is used [1]:

$$y(t_0) = A\int_0^{t_0} u^2(\tau)\partial\tau. \qquad (4)$$

It allows to calculate the maximum filter output signal at time $t = t_0$. If the spectrum of the signal is known and equal to $S(j\omega)$, then the optimum filter must have a transfer function:

$$H(j\omega) = \frac{S^*(j\omega)}{W(j\omega)}e^{-j\omega t_0}, \qquad (5)$$

where $S^*(j\omega)$ is a complex-conjugate function, t_0 - integration time, or time in which the signal/noise ratio is maximized.

The main types of noise in photoelastic microscope are: laser noise, modulator noise, photodetector noise, amplifier noise and structural noise.

The main noise of the laser according to [5] consists of quantum noise, current distribution noise, mods noise and backward reflection noise. Their calculation is a difficult task, but very easy to estimate experimentally by measuring the relative intensity noise (relative intensity noise - *RIN*). Let the laser emits an average power P, the output power of laser diode is fed through an optical scheme to a photodetector with current feedback $\rho_з$ and it is connected to a selective amplifier with wide bandwidth Δf. The average value of a experimentally measured current is equal to $\rho_з P$, and average value of squared noise current is $\overline{i_{LN}^2} = RIN(\rho_з P)^2 \Delta f$, if P_{LN} is a laser power then an expression for RIN of laser in photoelastic microscope with $\Delta f = 1{,}6$ kHz :

$$RIN = \frac{P_{LN}^2}{P^2 \Delta f} = \frac{\sqrt{\overline{i_{LN}^2}}}{\rho_i} = \frac{10}{\Delta f}\lg\frac{\delta\overline{P}}{\overline{P}} \approx -80 \pm 1 \text{ dBV}. \quad (6)$$

Theoretical calculation of S/N ratio ψ in photoelastic microscope gives the result (on the output of the photodetector in the bandwidth 1,6 kHz):

$$\psi = 10\lg\frac{P_{signal}}{P_{noise}} =$$

$$= 10\lg\left[\frac{(\rho_i P)^2 R}{2eR\Delta f\left(I_О + \rho_i P + 4kT\Delta f + RIN(\rho_i P)^2 \Delta f R\right)}\right] = \quad (7)$$

$$= 70 \pm 10 \text{ dB}$$

where $R = 10 \pm 5\%$ kilohms - photodetector load resistance, e - electron charge, I_T - photodetector dark current, $P = 25$ mW - average power of the laser, k - Boltzmann constant, T - absolute temperature.

Other noises are calculated using formulas that are described in detail in [6]. Shot noise according Schottky formula together with the background noise exposure and backward reflection noise is less than 10^{-10} W. Structural noise that occurs when positional system of photoelastic microscope works is tens of nanometers, and surface acoustic vibrations do not exceed fractions of a nanometer, that at the averaging time of 0.1 second and 1 micron per step allows them to be neglected.

Thus, the analysis of energy and spectral characteristics of noises [6] allows legitimately consid-ering the noise - white Gaussian noise. Selective signal measurement is made by nanovoltmeter at 50 kHz, with a bandwidth of 1.7 kHz. Using synhronous phase detection bandwidth is compressed to 1 kHz.

Accepting that the input signal of nanovoltmeter is $U_s(t) = U_s \cos(\omega_0 t)$ with additive white Gaussian noise $\xi(t)$, then input signal $U_{in}(t) = U_s(t) + \xi(t)$ after a multiplier gives a cross-correlation function:

$$
\begin{aligned}
R^*(\tau) &= \frac{1}{T}\int_0^T \left[U_{in}(t) + \xi(t) \right] \cdot U_0(t+\tau)\,dt = \\
&= \frac{1}{T}\int_0^T \left[U_{in} U_0 \cos(\omega_0 t)\cdot\cos\omega_0(t+\tau) + U_0 \cos\omega_0(t+\tau)\cdot\xi(t) \right]dt = \\
&= \frac{U_0 U_{in}}{2T}\int_0^T \left[\cos(\omega_0 t) + \cos\omega_0(2t+\tau)\right]dt + \frac{U_0}{T}\int_0^T \left[\cos\omega_0(t+\tau)\cdot\xi(t)\right]dt = \\
&= \frac{U_0 U_{in}}{2}\cos(\omega_0\tau) + \frac{U_0 U_{in}}{2T}\int_0^T \cos\omega_0(2t+\tau)\,dt + \frac{U_{in}}{T}\int_0^T \left[\cos\omega_0(t+\tau)\cdot\xi(t)\right]dt = \\
&= \frac{U_0 U_{in}}{2}\cos(\omega_0\tau) + \frac{U_0 U_{in}}{4\omega_0 T}\left[\sin\omega_0(2T+\tau) - \sin(\omega_0\tau)\right] + \frac{U_0}{T}\int_0^T \left[\cos\omega_0(t+\tau)\cdot\xi(t)\right]dt.
\end{aligned}
\tag{8}
$$

It is seen that the second term describes the behavior of the background at the end of integration time, and the third describes the noise. It is also clear that the impact of the background noise and illumination decreases with increasing the integration time. Knowing the spectral density of white Gaussian noise S_0, and transfer factor $K(j\omega) = \dfrac{\beta}{\beta+j\omega}$ of RC-filter, then its output correlation function is $B(\tau) = \dfrac{S_0 \beta}{2} e^{-\beta|\tau|}$. Thus the amplitude of the noise at the filter output will be:

$$
\sqrt{\overline{U_N^2}} = \frac{U_0 \sqrt{S_0}\,|K(j\omega_0)|}{\sqrt{\bar{O}}},
\tag{8}
$$

Taking into account the previous notation (4-8) the cross-correlation function of the signal will be:

$$
R_s(t) = \frac{U_{in} U_0}{2}|K(j\omega)|\cos(\omega_0\tau).
\tag{9}
$$

Thus the signal/noise ratio is calculated as:

$$
\psi \approx \frac{U_{in}\sqrt{T}}{2\sqrt{S_0}} = \frac{U_{out}}{\sqrt{\overline{U_N^2}}} = 20\lg\frac{U_{out}}{\sqrt{\overline{U_N^2}}} \approx 65 \pm 10\ dB.
$$

Where U_{out} - optimum filter output voltage from 1 mV to 1 V, T – correlation time. This is an important result: the accumulation of a periodic signal, which can occur for a number of periods, the signal/noise ratio at the output of the correlation filter increases proportionally to the square root of accumulation time (integration). It is clear that the resulting dependence of the signal/noise ratio from integration time will be the same in the case of complex periodic (pulsed) signal. Note that in this case, and the reference signal should have the same spectrum the signal itself.

Measurement errors of photoelastic microscope lay in the determination errors of Stokes parameters and accuracy of submicron positioning system (from 0,01% to 10%). Knowing the functional dependence of the output signal from the polarization ellipse parameters [18] the maximum error is calculated as:

$$
\frac{\Delta I_{out}}{I_{in}} = \sqrt{\left(\frac{\partial I(\theta_{\text{м}},\delta_0,\vartheta)}{\partial\theta_{\text{м}}}\right)^2 \Delta\theta_{\text{м}}^2 + \left(\frac{\partial I(\theta_{\text{м}},\delta_0,\vartheta)}{\partial\delta_0}\right)^2 \Delta\delta_0^2 + \left(\frac{\partial I(\theta_{\text{м}},\delta_0,\vartheta)}{\partial\vartheta}\right)^2 \Delta\vartheta^2} \approx 0{,}05,
$$

where $\Delta\theta_i = 10^{-7}$ rad, $\Delta\delta_0 = 10^{-5}$ rad, $\Delta\vartheta = 10^{-6}$ rad. $\Delta\theta_i$ is the angle error between the optical indicatrix of modulator and the sample, $\Delta\delta_0$ - the maximum phase shift error made by birefringence, $\Delta\vartheta$ - the initial error phase of laser radiation.

So developed photoelastic microscope used in this study has the following system of parameters:

- Modulation factor: 90 %;
- Supply voltage of quartz cavity: 40-50 V;
- The size of the cavity: 10x15x45 mm;
- The size of the active phase plate: 10x15x50mm;
- Sensitivity to change of phase modulated radiation: $\partial\varphi = 5 \cdot 10^{-6}$ rad;
- The range of wavelengths of laser radiation: λ=400–2000nm;
- Frequency of polarization modulation: 50-80kHz;
- Minimum positional sensitivity (determined by stepper motor): 10/1/0,5/0,1 μm;
- The minimum size of the laser scanning spot (limited by λ_{laser}): 0,4-5 μm;
- Maximum resolution (limited by λ_{laser}): 0,2-1μm;
- Maximum sensitivity to the relative change of the refractive index: 10^{-10};
- The optimal signal/noise ratio: 65 ± 10 dB;
- Maximum measurement errors: 15%.

2.2. Sample and device parameters

As a model object it was made a sample in the form of a plate with dimensions (mm) $l_x \times l_y \times l_z$=10×50×20, cut from the blank quartz glass, intended for the manufacturing of optical products. There were three equally important factors for the choice of material: the relatively small value of the heat conductivity coefficient that satisfies the condition of slow dynamics; the expected optical and mechanical homogeneity of the sample; and the uniqueness of the nature of the thermal conductivity in the used temperature range.

The sample was made according to the standard method of optical components manufacturing (cutting, grinding, polishing) with the additional operation - annealing on the last stage. Its mode: soaking at 500° C for 3 hours and further cooling with the stove. The choice of the minimum sample size l_x is validated the necessity of obtaining the thermal front in the geometry close to a plane that is parallel to the laser beam scanning the sample.

It was mounted on a pyroceramic substrate with a nickel-film resistor on its surface, which played the role of a heat source. The resistor area some exceeds the size of the plate's end surface (10x20 mm²) for the mounting of copper contacts, which were connected to a DC power source. Parameters of the resistor preset the power of heat source not more than 1W in the stationary mode. Fixation of the sample position on the resistor and the thermal contact with it was provided by the heat-conductive paste, which excluded the appearance of a stresses caused by the fastening conditions.

Scanning of the sample by the focused micron probe beam with wavelength 630 nm was made by turn along each of the axes with the help of the displacement device with step 10 microns, controlled by a stepper motor. The photodetector signal was measured by lock-in-nanovoltmeter, in which the value of integrating constant was established taking into account the dynamics inherent to the thermal process. Thus, weakly varying a parameter, its value could be increased by up to 3 seconds. If it was required to scan the strain/stress distribution in the sample by the probe beam, this value was set at 0.1s, the reproduction of the results under the variation of the integrating constant was a suitability criteria. Thus measurements were hold with S/N ratio equal to 60 dB.

The sensitivity of the measuring system, with respect to mechanical strain/stress was determined by comparing the signals from the radiation passed standard quarter-wave plate and an equivalent sample that was subjected to controlled value of uniaxial compressive force.

As it was expected, the condition $\varphi \ll 1$ was highly satisfied in our case, which gives the right for the application of the relation $l_v \approx \varphi$ in the range of measured value, covering 3 orders using the modern standard equipment.

The value of l_v was measured in three ways: 1 – as a function of y-position of the sample along the direction of heat flux in specific moments of its propagation, 2 – as a function of time at certain points in the same position, and 3 – as a function of the x-and z-positions at a fixed value of the y-position.

$T(t)$ and $T(y)$ were measured as an auxiliary with the use of a thermovision camera and a semiconductor detector for the comparison of the results that were obtained from measurements of the birefringence. All measurements were performed in air environment at atmospheric pressure and natural convection.

Note, that $T(t)$ and $T(y)$, obtained from measurements of the birefringence, are characteristics of current temperature change with respect to the op-

posite cold end of the sample. Due to these facts, measures had to be taken to eliminate the instability of natural air flows in the near-sample area, which were the source of low-frequency fluctuations in the measured signal.

3. Results

The measurement results obtained by first way are shown in fig. 2 in the form of the coordinate dependences of the anisotropy value in the sample, calibrated to the values of uniaxial strains/stresses: (a) in the initial state and after annealing, and (b) also at the presence of heat flow through the 1, 5 and 20 minutes after turning on the heat source. Since the magnitude of stress (deformation) in the
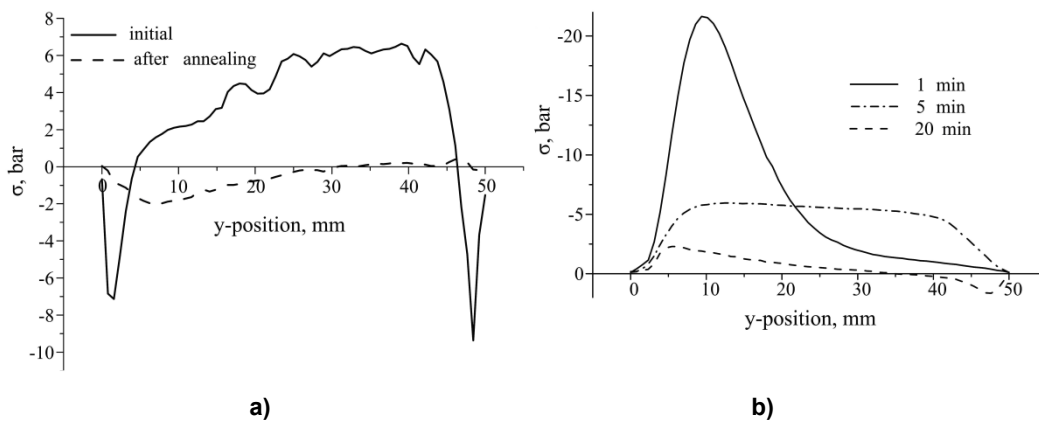
range of Hooke's law is a linear superposition of the values from different sources, the components that are induced by heat flux and are shown in fig. 2 (b) were determined as the difference betweenthe corresponding curves in the heating conditions and without it. The ordinates shown in fig. 2 (a) and 2 (b) give information about the ratio between the strain value in the initial and annealed state and stresses induced by the heat flow.

Several conclusions come from fig. 2 and they are following. The first implies that all substances in the condensed state are heterogeneous and therefore have a dielectric anisotropy which value depends on the detectivity of measuring devices as well as the degree of inhomogeneity.

Fig. 2. (a) – solid line shows the distribution of $\sigma(y)$ in the sample before annealing and dashed is after; (b) – the distribution of $\sigma(y)$ in the sample caused by heat flow generated by a 1W heater at different moments of time starting from turning on

Therefore, the homogeneity of the sample that has been found is two orders of magnitude lower than expected according to the detectability of the setup. However, an annealing, by analogy with the chemical etching, actually eliminates the surface tension by smoothing the internal heterogeneity and keeps the optical properties of the surface. Further, from the curve of strain distribution in the original sample, it can be concluded that the surface tension of the polished side surfaces of the sample is much lesser than grinded surfaces on its top and bottom. In both cases, the sign of the strain corresponds to compressive deformation, and the opposite signs in the distribution along the sample are related with 90° difference in orientation of the optical indicatrix, which is equivalent to the sign changing of difference $(n_x - n_y)$.

The measurement results received by second way are shown in fig. 3 as a dependence of mechanical stress value (anisotropy) on time, which is induced by heat flux along the y-position in the three fixed points.

Note that all relations of a starting point have origin of coordinates, rather than the strain value corresponding to the distribution $I_v(y)$ in fig. 2 (a). This is achieved by using an additional phase plate, which at the adjustment of appropriate azimuth compensates the initial signal. This procedure does not distort the measurement result and allows showing in details the dynamics of the heat transfer process at the start of heating. As it turned out, this dynamic is not without paradox in the sense that almost at any point in the sample along the y-axis the tension/stress appeared at the same time the heater was turned on.
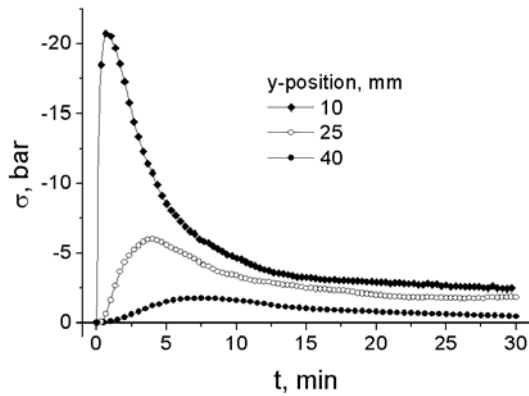
Fig. 3. The dynamics of σ(*t*) value at different points of the probe beam y-position

The reliability of the obtained results from the point of existing relation of signal-to-noise ratio is undisputed and the nature of its origin was described earlier.

4. The discussion of the results

Obtained results includes the fact that the amplitude of dependencies in figures 2 and 3 is determined by the value of $\mathrm{div}\left(\mathrm{grad}\right)\approx\sigma\left(y\right)$. It means that the stationary deformation of elastic solid induced by inhomogeneous temperature gradient is described by the Poisson equation, which in our system of coordinates is described as [18]:

$$\frac{\partial^2 u}{\partial y^2} = -\frac{\sigma\left(y\right)}{k} \qquad (10)$$

Here, u is a potential, related to the coordinate function of temperature (the Fermi energy, chemical potential), $\sigma\left(y\right)$ is the normal component of the mechanical strain/stress, and $1/k$ is a coefficient of proportionality. In the matter of complex composition, for example in semiconductor doped crystal, the role of the potential u fulfills the band gap energy. In this case, the internal mechanical strain/stress induced by the spatial inhomogeneity or defective structure of composition, is called a "frozen" thermoelasticity [13].

The presented experimental result in fig. 2 (b) is proportional to the right side of equation (10). This result can be used to solve the direct problems of nonstationary thermoelasticity which lay in obtaining $T(y)$ function. Its second derivative expresses the measurement result of the mechanical strain/stress. It is nessesary to solve the problem of non-stationary thermoelasticity with that fixed boundary conditions, which take place in our experiment. However, in the uncertainty conditions of heat transfer properties on the surfaces of the

sample searching of such a function is not only problematic, but doubtful expedient as well. It is much easier to get this function by dual operation of graphical integration of experimental dependences, providing a definiteness of integral by the corresponding conditions. The first condition is establishing the value of the constant component of the temperature function, which is determined by the difference of temperature values at the end of the sample and is lost during differentiation. The second condition establishes the connection of the second derivative value of the ordinate and the functions of mechanical strain/stress. Both conditions are met by additional one-time measurements that play the role of boundary conditions during the integration of differential equations.

Fig. 4 shows the result of processing the curve (1 min) from fig. 2 in comparison with the $T(y)$ function, obtained by measuring the temperature during the leaser beam displacement on *x-z*-surface along the plate.
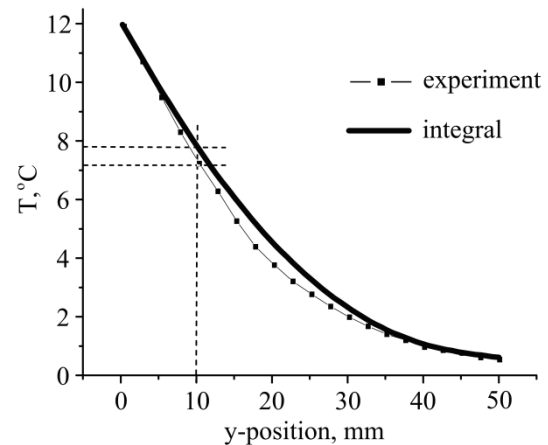

Fig. 4. The distribution of T(*y*), obtained by double integration of $\sigma\left(y\right)$ function shown in fig. 2 (b) and by its measuring at *y-x*-surface at t=1 min

The only adjustable parameter was the value of the constant component added to the result of the first integration, and the criterion of truth is the coincidence of the curves' values at the opposite ends of the sample. The quality of the characteristics consent can be discussed with a view to closeness of their monotonic trends, which is quite satisfactory. Because, in fact, each of them belongs to different objects – the volume and surface, their temperatures for various reasons may differ by several degrees. For this reason, the question of the truth of the absolute values of the curves is not observed in this case, furthermore, being coordinated in the trend the measuring data received by thermal imager has significantly different amplitudes.

For this reason, the question of the truth of the absolute values of the curves in this case is not observed, all the more to point that going with the tendency, received by thermal imager the measuring data has significantly different values of amplitude. The lateral distribution of $\sigma(y)$ shown in fig. 5 differs from the longitudinal with the fact that it has amplitudes comparable in magnitude with opposite signs. And the sign of stress/strain in the middle of the sample coincides with the distribution $\sigma(y)$, which is natural, because at the same parameters of space-time the amplitudes must coincide. As for the presence of stress with "positive" sign, first of all, its origin is the reaction of an elastic medium in the surface region on the stress/strain of the volume with "negative" sign.
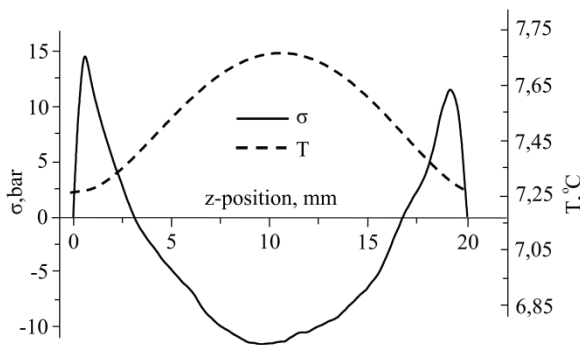

Fig. 5. The distribution of *T(z)*, **obtained by double integration of the function** $\sigma(z)$ **at y=10 mm**

Secondly, the component of the heat flux normal to the surface creates a temperature function with a curvature of opposite sign with respect to volume (dashed curve in fig. 5). This function, as shown in fig. 4, was obtained by double integration of $\sigma(z)$ with the difference that according to symmetry of experiment conditions the temperature difference was determined not by the ends of a sample, but by its values on the surface and inside the sample. The last was determined from $\sigma(y)$ at y = 10 mm at the probe position of lateral distribution from fig. 4. To the point, the distribution of $\sigma(x)$ (not shown) differs from fig. 5 mainly by value of the scan coordinate.

For the interpretation of the results shown in fig. 3, it is assumed that the left side of equation (10) and the equation describing the process of heat conduction

$$\frac{\partial^2 T}{\partial y^2} = \frac{1}{D}\frac{\partial T(y)}{\partial t}, \tag{11}$$

are equal.

To express potential u as the temperature $T(y)$ and put into an equation (10), the expression is received subject to the marked circumstance:

$$\frac{\partial T}{\partial t} = k \cdot \sigma, \tag{12}$$

where k is proportionality coefficient.

From this equation follows that integrating of the functions $\sigma(t)$ it can be received an average temperature of across the sample section under the condition that integral is definite. This condition consists of the selection of a constant component for the experimental function of such magnitude, with regard to that the result of integration becomes a monotonic function corresponding to the real situation.

The result obtained by processing of the three curves from fig. 3 is shown in fig. 6 (a). For comparison, fig. 6 (b) shows the dependences of $T(t)$, obtained by using a semiconductor microthermometer under the same conditions. On the background of qualitative agreement in the trends of three pairs of curves there is a discrepancy, a possible cause of which may be at least two circumstances.

One of them consists in the fact that in equation (11) a component should be taken into account that is associated with the dissipation of thermal energy. Its nature consists in radiative and convective losses. The second circumstance is not so much in the quality of surface temperature displayed by microthermometer, as in the difference of its magnitude from the bulk value.

Note that the potion of the extremes in each of the curves in fig. 3 according to equation (10) shows localization of maximum curvature of the T(y) dependence that is observed at the corresponding positions of the sample (y = 10, 25, 40 mm). Since all three functions $T(t)$ are monotone according to experimental conditions, in this case the coordinate of a single extreme can be a sign of the heat wavefront and its dynamic information can be obtained from the relations $y_{\sigma max}(t)$. Indeed, there is a linear relationship between the positions of the extremes on the time scale and the values of the y-coordinates at which the dependence $\sigma(t)_{max}$ is registered. Thus, the velocity of heat flow can be judged by the magnitude of the slope coefficient of the linear dependence of $y_{\sigma max}(t)$.

Besides, the presence of a marked linear relation provides a basis for conclusion about the independence of the thermal conductivity as well as all the other coefficients involved in the process from the temperature in the operating range.
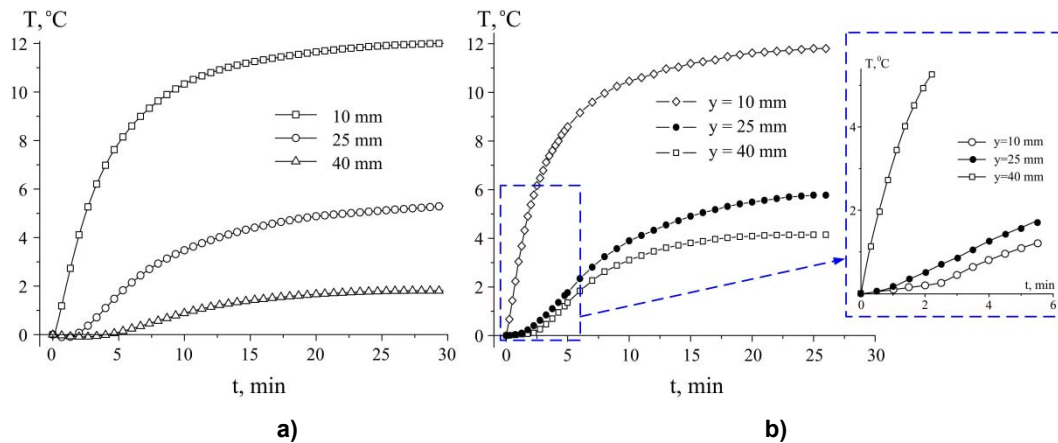

Fig. 6. The distributions of T(*t*) in three points of y-position, obtained by measuring the *y-x*-surface (a) and by double integration of $\sigma(t)$ function shown in fig. 3 (b)

Finally, there is the question about the participation of radiation component in the heat transfer. As already mentioned, a tangible criterion of its presence is the signal appearance in remote points from the heat source in the direction of the temperature gradient almost simultaneously with the resistor turning on. Having a look on the inset in fig. 6 (b) it becomes clearly that the dependence $\sigma(t)_{y=40}$ is especially representative in this sense, where the linear part of the mechanical strain/stress growth is uniquely related to the temperature increase of heating resistor. In addition, close emission and absorption spectra location of the heater and the glass assist to the effect of radiation nature of heat transfer in this case, although the source of radiation can be more heated part of the sample. The clarification of the circumstances connected to the observed phenomenon deserves a special consideration.

5. Conclusions

Modulation polarimetry (MP) represents a new approach to improving the birefringence measurement, which gives direct information about photoelastic and thermoelastic state of the material.

Using MP allowed to detect dynamics of optical anisotropy induced by thermal flow trough the sample with resolution $\Delta n/n = 10^{-10}$ [15]. Mechanical strains/stresses are experimentally measured in the plate-sample made of quartz glass using the photoelastic microscope, which are accompanied in time and space by the heat flow from the external source of heat. The modification of traditional PM method gave a resolution with respect to the magnitude of thermoelasticity, which allowed registering of limited temperature differences of few degrees. It is shown that the extremum of the function $\sigma(t)_{max}$ can be a sign of the thermal front, and information about the dynamics of heat flow can be obtained from the space-time dependences of the function extremum $\sigma(t)$. From measured functions $\sigma(y,t)$, at certain moments of time and in certain coordinates in the direction of heat flow the functions $T(y,t)$ were received by graphical integration which are in good agreement with experimental data. The high detectability of the devise is demonstrated on the detection of heat transfer component of radiation nature, whose source can be detected in both, the external heater and the sample.

In conclusion, photoelastic microscope appears to be a promising direction of polarimetry, ellipsometry, microscopy and other optical applications. The integration procedure of the experimental functions used in the work to solve the inverse problem of determining of thermal strains/stresses deprives the received result of errors up to 15% associated with spatial and temporal fluctuations caused by the experiment imperfection that always have a place. In comparison with existing devices and experimental setups [2-4, 7, 9-12,14,20] the presented photoelastic microscope show better detectability, more wide range of wavelengths and higher modulation frequency, also a metrological value is approved. It is established a direction of next improvements: scanning speed, software update, reaching a higher S/N ratio on the base of present-

ed and future theoretical and experimental researches.

References

1. *Алиев Т. М., Тер-Хачатуров А. А.* Измерительная техника: Учеб. пособие для тех. вузов. – М.: Высш.шк., 1991.- 383 с.: ил.

2. *Becchetti M., Flori R., Marsili M., Moretti M.* Comparison between Digital Image Correlation and Thermoelasticity for Strain Field Analysis // AIP Conf. Proc. – 2010. – Vol.1253, pp. 233-240.

3. *Becchetti M., Flori R., Marsili R., Rossi G. L.* Stress and strain measurements by image correlation and thermoelasticity // Proc. of the SEM Annual Conference. – 2009. – Pp. 1-6.

4. *Bhushan Bharat, Fuchs Harald (Eds.)* Applied Scanning Probe Methods II. Scanning Probe Microscopy Techniques. / Berlin: Springer-Verlag Heidelberg. –2006. – Pp. 321-357.

5. *Чадюк В. О.* Оптоелектроніка: від макро до нано. Генерація оптичного випромінювання: навч. Посіб. У 2 кн. / В. О. Чадюк. – К.: НТУУ «КПІ», 2012. – Кн. 2. – 436 с.

6. *Денбновецький С. В., Лещишин О. В.* Електронні системи: навч. Посіб. – К. НТУУ «КПІ», 2011. – 288с.

7. *Dulieu-Barton J. M., Stanley P.* Development and applications of thermoelastic stress analisys // J. of strain analisys. – 1998. – Vol. 33. no. 2. Pp. 93-104.

8. *Fofanov Ya. A.* Threshold Sensitivity in Optical Measurements with Phase Modulation // Proc. SPIE (The Report of tenth Union Simp. and Seminar on High-Resolution Molecular Spectroscopy) ed L.N. Siniza. – 1991. – Vol. 1811. Pp. 413-414.

9. *Gilmour I. W., Trainor A., Haward R. N.* Calculation of the Grüneisen constant of glassy polymers from thermoelastic data // J. of Polymer Science: Polymer Physics Edition. –1978. – Vol. 16. Pp. 1291-1295.

10. *Green A. E. and Lindsay K. A.* (Eds.) Thermoelasticity // J. of elasticity. – 1972. – Vol. 2, №. 1. –Pp. 1-7.

11. *Harwood N., Cummings W. M.* (Eds.) Thermoelastic Stress Analysis // Bristol: IOP Publishing Ltd. – 1991. – P. 400.

12. *Kasai M., Sawada T. (Eds.)* Photoacoustic and Photothermal Phenomena II // Berlin: Springer Verlag. – 1990. – Vol. 62. Pp. 33–36.

13. *Kovalenko A. D.* Thermoelasticity (Translated from the Russian by D. B. Macvean. With an appendix on Thermoelastic stability by J. B. Alblas). Groningen: Wolters-Noordhoff. – 1969. – P. 256.

14. *Mackin T. J., Roberts M. C.* Evaluation of damage evolution in ceramic-matrix composites using thermoelastic stress analysis // J. of the American-Ceramic-Society. – 2000. – Vol. 83, №. 2. Pp. 337-343.

15. *Oliinyk O., Tsyganok B., Serdega B., Matiash I.* Investigation of nonstationary thermo-photo-elastic effect using the polarization modulation of radiation // Proc. of the 34th Int. Spring Seminar on Electronics (IEEE Xplore). – 2011. – Pp. 294-298.

16. Пат. 74814 UA, МПК G01N 21/41 (2006.01) Спосіб для фотопружної мікроскопії твердих тіл та їх структур / О. О. Олійник, Б. А. Циганок, Б.К. Сердега; заявник і правовласник НТУУ «КПІ». — №. U201205269; заявл. 27.04.2012 ; опубл. 12.11.2012, Бюл. № 21.

17. Пат. 78510 UA, МПК G01N 21/41 (2006.01) Пристрій для фотопружної мікроскопії твердих тіл та їх структур / О. О. Олійник, Б. А. Циганок, Б.К. Сердега; заявник і правовласник НТУУ «КПІ». — №. U201209377; заявл. 31.07.2012 ; опубл. 25.03.2013, Бюл. № 6.

18. *Б. К. Сердега.* Модуляційна поляриметрія // К.: Наук. Думка. – 2011. – с. 238.

19. *Weber W.* Über die spezifische Wärme fester Körper insbesondere der Metalle Annalen der Physik und Chemie. – 1830. – Vol. 96. Pp. 177-213.

20. *Yao Nan, Wang Zhong Lin (Eds.)* Handbook of Microscopy for Nanotechnology. – 2005. – NEW YORK: KLUWER ACADEMIC PUBLISHERS.– Pp. 183-205.

I.Є. Матяш[1], канд.фіз.-мат.наук, **I.A. Міняйлова**[1], **О.М. Міщук**[1], канд.фіз-мат.наук, **О.О. Олійник**[2],
Б.К. Сердега[1], д-р фіз-мат. наук, **Б.А. Циганок**[2], канд.техн.наук

[1]Інститут фізики напівпровідників ім. В. Лашкарьова НАН України,
проспект Науки 45, Київ, 03028, Україна.
[2]Національний технічний університет України "Київський політехнічний інститут",
проспект Перемоги 37, Київ-56, 03056, Україна.

Детектування індукованих тепловим потоком напружень в твердому тілі за допомогою фотопружного мікроскопу

Мета цієї статті полягає в представленні переваг практичного та ефективного методу модуляційної поляриметрії (МПМ), застосованого до зразка кварцового скла у вигляді пластини для виявлення його найменших внутрішніх термонапружень, викликаних поширення теплової хвилі. Описаний МПМ дозволив провести точні вимірювання двопроменезаломлення, яке супроводжує динаміку термопружності, що зробило можливим обчислення значення розподілу напружень вздовж і поперек напрямку теплового потоку в певні моменти часу, а також їх залежність від часу в певних координатах теплового потоку. Основна мета даної роботи є не тільки вирішення обернених задач нестаціонарної термопружності, що дозволяє отримати просторово-часові температурні функції графічним інтегруванням експериментальних характеристик, але й дослідження динаміки точки максимуму кривизни температурної функції T(t), що є характеристикою теплового фронту в процесі встановлення теплового потоку . Окрім того, було показано, що завдяки високій виявній здатності МПМ застосованої у фотопружному мікроскопі, стало можливим спостерігати радіаційну складову теплопереносу. Бібл. 20 , рис. 5 .

***Ключові слова:** модуляційна поляриметрія, двопроменезаломлення, тепловий потік, термопружність, фотопружний мікроскоп.*

И.Е. Матяш[1], канд.физ.-мат.наук, **И.А. Миняйлова**[1], **А.М. Мищук**[1], канд.физ-мат.наук,
О.О. Олийник[2], **Б.К. Сердега**[1], д-р физ-мат. наук, **Б.А. Цыганок**[2], канд.техн.наук

[1]Институт физики полупроводников им. В. Лашкарева НАН Украины,
проспект Науки 45, Киев, 03028, Украина.
[2]Национальный технический университет Украины " Киевский политехнический институт",
проспект Победы 37, Киев -56, 03056, Украина.

Детектирование индуцированных тепловым потоком напряжений в твердом теле с помощью фотоупругого микроскопа

Цель этой статьи заключается в представлении преимуществ практического и эффективного метода модуляционной поляриметрии (МПМ), примененного к образцу кварцевого стекла в виде пластины для выявления его самых малых внутренних термонапряжений, вызванных распространением тепловой волны. Описанный МПМ позволил провести точные измерения двулучепреломления, которое сопровождает динамику термоупругости, что сделало возможным вычисление значения распределения напряжений вдоль и поперек направления теплового потока в определенные моменты времени, а также их зависимость от времени в определенных координатах теплового потока. Основная цель данной работы является не только решение обратной задачи нестационарной термоупругости, что позволяет получить пространственно-временные температурные функции графическим интегрированием экспериментальных характеристик, но и исследование динамики точки максимума кривизны температурной функции T(t), что является характеристикой теплового фронта в процессе установления теплового потока. Кроме того, было показано, что благодаря применению высокой обнаружительной способности МПМ в фотоупругом микроскопе сделало возможным наблюдать радиационную составляющую теплопереноса. Библ. 20, рис. 5 .

Ключевые слова: *модуляционная поляриметрия, двулучепреломление, тепловой поток, термоупругость , фотоупругий микроскоп.*

Список использованных источников

1. *Alyev T. M., Ter-Hachaturov A. A.* (1991), "Yzmerytel'naja tehnyka: Ucheb. posobye dlja teh. Vuzov". M., Vyssh. shk. P.383. (Rus).
2. *Becchetti M., Flori R., Marsili M., Moretti M.* (2010), "Comparison between Digital Image Correlation and Thermoelasticity for Strain Field Analysis" // AIP Conf. Proc. Vol.1253, pp. 233-240.
3. *Becchetti M., Flori R., Marsili R., Rossi G. L.* (2009), "Stress and strain measurements by image correlation and thermoelasticity" // Proc. of the SEM Annual Conference, pp. 1-6.
4. *Bhushan Bharat, Fuchs Harald (Eds.)* (2006), "Applied Scanning Probe Methods II. Scanning Probe Microscopy Techniques" // Berlin: Springer-Verlag Heidelberg, pp. 321-357.
5. *Chadjuk V. O.* (2012), „Optoelektronika: vid makro do nano. Generacija optychnogo vyprominjuvannja: navch. Posib. U 2 kn." / V. O. Chadjuk. – K.: NTUU «KPI»,. -Kn. 2. P. 436. (Ukr).
6. *Denbnovec'kyj S. V., Leshhyshyn O. V.* (2011), Elektronni systemy: navch. Posib. – K. NTUU «KPI». P. 288. (Ukr).
7. *Dulieu-Barton J. M., Stanley P.* (1998), "Development and applications of thermoelastic stress analisys", J. of strain analisys Vol. 33. no. 2. pp. 93-104.
8. *Fofanov Ya. A.* (1991), "Threshold Sensitivity in Optical Measurements with Phase Modulation" Proc. SPIE (The Report of tenth Union Simp. and Seminar on High-Resolution Molecular Spectroscopy) ed L.N. Siniza. Vol. 1811, pp. 413-414.
9. *Gilmour I. W., Trainor A., Haward R. N.* (1978), "Calculation of the Grüneisen constant of glassy polymers from thermoelastic data", J. of Polymer Science: Polymer Physics Edition. Vol. 16, pp. 1291-1295.
10. *Green A. E. and Lindsay K. A.* (Eds.) (1972), "Thermoelasticity" J. of elasticity Vol. 2, no. 1, pp. 1-7.
11. *Harwood N., Cummings W. M.* (Eds.) (1991), "Thermoelastic Stress Analysis" (Bristol: IOP Publishing Ltd.). P. 400.
12. *Kasai M., Sawada T. (Eds.)* (1990), "Photoacoustic and Photothermal Phenomena II" (Berlin: Springer Verlag) Vol. 62, pp. 33–36.
13. *Kovalenko A. D.* (1969), "Thermoelasticity" (Translated from the Russian by D. B. Macvean. With an appendix on Thermoelastic stability by J. B. Alblas). Groningen: Wolters-Noordhoff. P. 256.
14. *Mackin T. J., Roberts M. C.* (2000), "Evaluation of damage evolution in ceramic-matrix composites using thermoelastic stress analysis", J. of the American-Ceramic-Society, Vol. 83, no. 2, pp. 337-343.
15. *Oliinyk O., Tsyganok B., Serdega B., Matiash I.* (2011), "Investigation of nonstationary thermo-photo-elastic effect using the polarization modulation of radiation" Proc. of the 34th Int. Spring Seminar on Electronics (IEEE Xplore), pp. 294-298.
16. *O. Olijnyk O., Tsyganok B. A., B.K. Serdega.* Pat. №74814 Ukrai'na "Sposib dlja fotopruzhnoi' mikroskopii' tverdyh til ta i'h struktur"; zajavnyk i pravovlasnyk NTUU «KPI». № u201205269; zajavl. 27.04.2012; opubl. 12.11.2012, Bjul. №21. (Ukr)
17. *O. O. Olijnyk, B. A. Tsyganok, B.K. Serdega* Pat. №78510 Ukrai'na, "Prystrij dlja fotopruzhnoi' mikroskopii' tverdyh til ta i'h struktur"; zajavnyk i pravovlasnyk NTUU «KPI». № u201209377; zajavl.31.07.2012; opubl. 25.03.2013, Bjul. № 6. (Ukr)
18. *Serdega B. K.* (2011), "Moduljacijna poljarymetrija".K. Nauk. Dumka. P. 238 (Ukr)
19. *Weber W.* (1830), "Über die spezifische Wärme fester Körper insbesondere der Metalle Annalen der Physik und Chemie" Vol. 96, pp. 177-213.
20. *Yao Nan, Wang Zhong Lin (Eds.)* (2005), "Handbook of Microscopy for Nanotechnology". NEW YORK: KLUWER ACADEMIC PUBLISHERS, pp. 183-205.